IEEE Transactions on Wireless Communications, Volume 21, Issue 10, October 2022, pp. 7881-7896
DOI:10.1109/TWC.2022.3162722

Two-timescale Resource Allocation for Automated Networks in IIoT

Yanhua He, *Member, IEEE*,Yun Ren, Zhenyu Zhou, *Senior Member, IEEE,* Shahid Mumtaz, *Senior Member, IEEE,* Saba Al-Rubaye, *Senior Member, IEEE,* Antonios Tsourdos, *Member, IEEE,* and Octavia Dobre, *Fellow, IEEE*.

Abstract

The rapid technological advances of cellular technologies will revolutionize the network automation, laying the foundation for realizing industrial Internet of things (IIoT) . In this paper, we investigate the two-timescale resource allocation problem in IIoT networks with hybrid energy supply. In such a system, the temporal variations of energy harvesting (EH), electricity price, channel state, and data arrival exhibit different granularity. The formulated resource allocation problem consists of energy management at large timescale, as well as rate control, channel selection, and power allocation at small timescale. To address this challenge, we combine Lyapunov optimization, alternating direction method of multipliers (ADMM), and matching theory to develop an online solution, which guarantees bounded performance deviation with only causal information. Specifically, Lyapunov optimization is leveraged to transform the long-term stochastic optimization problem into a series of short-term deterministic optimization problems. Then, a low-complexity rate control algorithm is developed based on ADMM, which accelerates the convergence speed via the decomposition-coordination approach. Next, the joint channel selection and power allocation problem is transformed into a one-to-many problem, and solved by the proposed price-

Y. He and Y. Ren are with the State Grid Zhejiang Electric Power Company Ningbo Bureau, Zhejiang, China (E-mail: yanhuahe91927@163.com, ren_yun@zj.sgcc.com.cn).

Z. Zhou is with the School of Electrical and Electronic Engineering, North China Electric Power University, Beijing 102206, China (E-mail: zhenyu_zhou@ncepu.edu.cn).

Z. Zhou is the corresponding author.

S. Mumtaz is with the Instituto de Telecomunicações,1049-001 Aveiro, Portugal (E-mail: smumtaz@av.it.pt).

S. Al-Rubaye and A. Tsourdos are with the School of Aerospace, Transport and Manufacturing, Cranfield University, UK (E-mail: s.alrubaye@cranfield.ac.uk, a.tsourdos@cranfield.ac.uk).

O. Dobre is with the Faculty of Engineering and Applied Science, Memorial University, Newfoundland, Canada (E-mail: odobre@mun.ca).

Published by IEEE. This is the Author Accepted Manuscript issued with: Creative Commons Attribution Non-Commercial License (CC:BY:NC 4.0).
The final published version (version of record) is available online at DOI:10.1109/TWC.2022.3162722. Please refer to any applicable publisher terms of use.

based matching with quota restriction. Finally, the proposed algorithm is verified through simulations under various system configurations.

Index Terms

Automated network, IIoT, two-timescale resource allocation, Lyapunov optimization, one-to-many matching, ADMM.

I. Introduction

A. Background and Motivation

Automated networks relies on seamless integration of advanced self-optimized techniques to improve efficiency, reliability, and operation economics for industrial Internet of things (IIoT) applications. In such a paradigm, billions of IIoT devices will be deployed in the industrial sector, and huge volume of data has to be transmitted on a real-time basis [1]. Fifth-generation (5G) cellular technologies provide more resilient network infrastructure for connecting the massive number of IIoT devices. However, carbon dioxide generated by powering the cellular infrastructures puts a tremendous pressure on the environmental as well as raise doubts about the sustainability of 5G-empowered IIoT networks [2]. Faced with the urgent need of green cellular networks for supporting various IIoT applications, researchers have focused on energy-saving strategies both on data transmission side and energy supply side.

On the data transmission side, network sleeping mode [3] and energy-efficient resource allocation techniques [4] are widely mentioned, applied and continuously improved. On the energy supply side, harvesting renewable energy such as solar and wind energy is advocated to power base stations (BSs) [5]. However, renewable energy sources with intermittent and fluctuating characteristics cannot provide reliable quality of service (QoS) guarantees. A more feasible approach is to utilize both unreliable renewable energy sources and reliable grid power in a complementary manner [6], [7]. In this sense, the coexistence of various energy sources further complicates the resource allocation problem in 5G-empowered IIoT networks. There exist several challenges that remain unsolved.

First, energy resource allocation and communication resource allocation are intertwined with each other and should be jointly optimized. The formulated joint optimization problem is generally NP-hard due to the coupling between energy and communication domains. Second, energy harvesting (EH), electricity price, channel state, and data arrival all exhibit high temporal-spatial

dynamics [8], which may have different granularity. Generally, the former two change in large timescale such as minutes [9], while the latter two change in small timescale such as seconds or even milliseconds [10]. How to optimize resource allocation under multi-dimensional randomness with different timescales is still an open issue. Third, the optimization of communication resource allocation involves long-term cooperation between different layers, e.g., rate control in the network layer and power allocation in the physical layer. In such a long-term cross-layer resource allocation paradigm, the coupling of strategies among different time slots as well as the coupling between physical and upper layers are neglected in most existing works, which focus on either performance optimization of a single layer, or the short-term deterministic optimization. Last but not least, the large-scale deployment of IIoT devices brings new scalability issues. The strategies of different devices are coupled together due to the constraint of sum rate or sum power consumption, which leads to prohibitive computational complexity when the number of devices is large.

Powering cellular networks with renewable energy sources has attracted intensive attentions from both industry and academia [11]. In [12], Zhang *et al.* proposed several energy-aware traffic offloading schemes to make efficient use of the harvested energy for reducing grid energy consumption. In [13], Doost *et al.* optimized the policy of downlink scheduling for EH-based cellular networks. Nevertheless, these research attempts mainly target at single-timescale resource allocation, and ignore the different time granularity of the above-mentioned stochastic processes.

There are some works taking different time granularity into consideration. In [14], Gong *et al.* studied the timescale difference between energy arrival variation and channel fading, and proposed a low-complexity two-stage joint power allocation and energy management optimization algorithm based on Markov decision process (MDP) and dynamic programming. In [15], Liu *et al.* investigated the minimization of on-grid energy consumption from both the space and time dimensions, and developed a low-complexity offline algorithm based on non-causal information as well as several heuristic online algorithms based on only causal information. However, both [14] and [15] rely on the assumption that the uncertainties follow some well-known probability distribution. They are not suitable for the scenario where the practical probability distributions of uncertain factors disagree with the pre-assumed statistical models. Actually, in real-world implementation, even the knowledge of statistical information is difficult to be identified.

Lyapunov optimization allows a distribution-free model of stochastic processes and provides bounded performance guarantees under all possible realizations of uncertainties [16]. It has

been widely applied for resource allocation optimization in time-varying wireless networks [17], hybrid energy powered green cellular networks [18], and EH-based two-way relay cooperative networks [19], etc. Nevertheless, the above-mentioned works mainly focus on one-timescale stochastic models, and cannot be directly applied to solve the two-timescale resource allocation problem addressed in this paper. Moreover, they cannot well handle the large-scale optimization problem with massive number of IIoT devices, because the computational complexity grows rapidly with the number of devices due to the coupling of strategies across different devices.

B. Contribution

Motivated by these gaps, we propose a two-timescale resource allocation algorithm for 5G-empowered automated networks that apply in IIoT by combining Lyapunov optimization, alternating direction method of multipliers (ADMM), and matching theory. The main objective is to maximize the long-term network utility via the joint optimization of communication resources and energy resources. First, we establish both data queue and energy queue in different timescales. The joint optimization problem is formulated as a long-term reward-plus-penalty problem, in which the network quality of experience (QoE) is taken as the reward while the energy purchasing cost is taken as the penalty. Then, the long-term stochastic optimization problem is further converted to a short-term deterministic optimization problem and decomposed into several subproblems with different timescales by leveraging Lyapunov optimization. Next, by opportunistically minimizing the upper bound of drift-minus-utility, the separated energy management, rate control, as well as joint channel selection and power allocation subproblems are solved sequentially by using linear programming, ADMM, and price-based one-to-many matching, respectively.

The main contributions are summarized as follows.

- *Two-timescale resource allocation with bounded performance deviation:* The proposed algorithm consists of the optimization of energy management at large timescale, as well as the optimization of rate control, channel selection, and power allocation at small timescale. It can guarantee bounded deviation from the optimum performance without requiring any prior knowledge of future channel state information (CSI), EH, and electricity prices.
- *Low-complexity rate control based on ADMM:* We develop an ADMM-based low-complexity rate control algorithm for the scenario with massive number of IIoT devices. It significantly reduces computational complexity by decomposing the large-scale optimization problem

into a series of subproblems with lower complexity, and accelerates the convergence speed via effective coordination of subproblem solutions.

- *Joint channel selection and power allocation based on matching:* The coupling between channel selection and power allocation is resolved by transforming the joint optimization problem into a one-to-many matching problem, which is then solved by the proposed price-based matching algorithm with quota restriction.
- *Comprehensive theoretical analysis and performance validation:* We provide a comprehensive theoretical analysis for the proposed algorithm in terms of optimality, convergence, and complexity. Intensive simulation results are conducted under different scenarios to demonstrate its performance gains.

C. Organization

The rest of this paper is organized as follows. System model is described in Section II. Problem formulation is provided in Section III. Section IV elaborates the proposed two-timescale resource allocation algorithm. A comprehensive property analysis is provided in Section V. Numerical results and analysis are introduced in Section VI. Finally, the conclusion is summarized in Section VII.

II. System model

We consider the downlink scenario of a hybrid energy powered cellular network for IIoT as shown in Fig. 1. The BS provides wireless connection and data transmission for the IIoT devices within its coverage. It is connected with a rechargeable battery, which supplements energy by either harvesting energy from external renewable energy sources, or purchasing energy from the power grid. The energy supply volatility caused by intermittent renewable energy sources is compensated by the reliable grid power. In addition, the BS maintains a data buffer to store the burst traffic flow towards the IIoT devices. In the following, the models of timescale difference, data queue, and energy queue are introduced in details.

A. The Model of Timescale Difference

Fig. 1 shows the timescale difference between data arrival and energy arrival. The two-timescale model proposed in [8], [20] is adopted, where the continuous time dimension is partitioned into successive identical data slots with slot duration T_0 seconds, which is indexed by

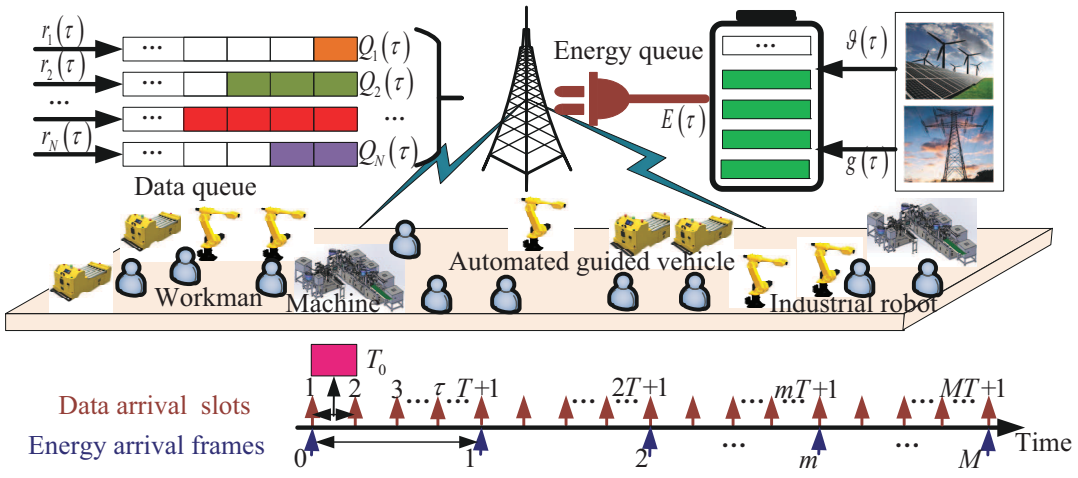


Fig. 1. Automated networks with hybrid energy supply for IIoT applications.

$\tau = 1, 2, \cdots, MT$. Since energy arrival changes much slower than data arrival, we can assume that energy arrival remains constant during T ($T >> 1$) data slots. Therefore, T data slots are grouped as an energy frame with duration of TT_0 seconds, which is indexed by $m = 1, 2, \cdots, M$.

B. The Model of Data Queue

Let $\mathcal{N} = \{1, 2, \cdots, n, \cdots, N\}$ and $\mathcal{K} = \{1, 2, \cdots, k, \cdots, K\}$ denote the sets of IIoT devices and channels, respectively. Let $r_n(\tau)$ denote the amount of data arriving at the BS's network layer per second for device n at data slot τ, which is firstly stored in an infinite buffer before transmission. The experience of device towards the service quality can be characterized by quality of experience (QoE) [21]. We assume that the QoE of device n, i.e., $U_n(\tau)$, is positively related to the amount of admitted data, which is given by

$$U_n(\tau) = \chi_n \log_2 [1 + r_n(\tau)] \tag{1}$$

Here, χ_n is a service weight parameter which indicates the importance or priority of $r_n(\tau)$ to the QoE of device n. Intuitively, device n with a larger χ_n prefers higher admission rate $r_n(\tau)$ because $U_n(\tau)$ increases more rapidly with $r_n(\tau)$ when χ_n is large. The logarithmic function represents that the marginal increment of QoE declines gradually with $r_n(\tau)$.

Let $x_{n,k}(\tau) \in \{0,1\}$ be the channel selection index. When $x_{n,k}(\tau) = 1$, the downlink signal to noise ratio (SNR) of device n over channel k is given by

$$\gamma_{n,k}(\tau) = \frac{p_{n,k}(\tau) h_{n,k}(\tau)}{\sigma^2} \tag{2}$$

where $p_{n,k}(\tau)$ is denoted as the transmission power allocated to device n over channel k at data slot τ. $h_{n,k}(\tau)$ is the channel gain between the BS and device n over channel k. σ^2 is the Gaussian white noise power.

Then, the downlink transmission rate $v_n(\tau)$ from the BS to device n can be derived according to the Shannon-Hartley theorem [22], i.e.,

$$v_n(\tau) = \sum_{k=1}^{K} x_{n,k}(\tau) B_k(\tau) \log_2[1 + \gamma_{n,k}(\tau)] \tag{3}$$

where $B_k(\tau)$ denotes the bandwidth of channel k.

The data buffered at the BS towards each IIoT device can be regarded as a data queue. Denote the data queue related to device n as queue n, where $r_n(\tau) T_0$ and $v_n(\tau) T_0$ can be regarded as the data input and data output of queue n, respectively. Particularly, $r_n(\tau) T_0$ indicates how much data should be sent to the BS in the view of the network layer at data slot τ and $v_n(\tau) T_0$ indicates how much data should be sent from the BS to device n via wireless link in the physical layer at data slot τ. Let $Q_n(\tau)$ denote the data backlog of queue n at data slot τ, which is evolved as

$$Q_n(\tau+1) = \max[Q_n(\tau) - v_n(\tau) T_0, 0] + r_n(\tau) T_0 \tag{4}$$

$Q_n(\tau)$ is mean rate stable [23] if $\lim_{\tau\to\infty} \frac{\mathbb{E}[|Q_n(\tau)|]}{\tau}=0$, which implies that the time-average data output is greater than or equal to the time-average data input, i.e.,

$$\lim_{M\to\infty} \frac{1}{MT} \sum_{\tau=1}^{MT} v_n(\tau) \geq \lim_{M\to\infty} \frac{1}{MT} \sum_{\tau=1}^{MT} r_n(\tau) \tag{5}$$

The network is considered to be mean rate stable if $\lim_{\tau\to\infty} \frac{\mathbb{E}[|Q_n(\tau)|]}{\tau}=0$ holds for any device $n \in \mathcal{N}$.

In addition, the time-average communication delay d_n after the n-th queue stabilizes is taken into account [24], which is given by

$$d_n = \frac{\lim_{M\to\infty} \frac{1}{MT} \sum_{\tau=1}^{MT} r_n(\tau)}{\left\{\lim_{M\to\infty} \frac{1}{MT} \sum_{\tau=1}^{MT} v_n(\tau)\right\} \left\{\lim_{M\to\infty} \frac{1}{MT} \sum_{\tau=1}^{MT} [v_n(\tau) - r_n(\tau)]\right\}} \leq d_n^* \tag{6}$$

where d_n^* is the upper bound of delay for device n.

Remark 1: Since data arrival and CSI vary across different data slots, the BS has to schedule the values of $r_n(\tau)$, $x_{n,k}(\tau)$, and $p_{n,k}(\tau)$ for each device $n \in \mathcal{N}$ every data slot.

C. The Model of Energy Queue

The BS can either exploit the renewable energy or purchase the grid power. Denote the harvested energy at data slot τ as $\vartheta(\tau)$, which satisfies the following EH constraint

$$0 \leq \vartheta(\tau) \leq \Phi(\tau) \tag{7}$$

where $\Phi(\tau)$ denotes the upper bound of harvested energy, which also changes randomly. Denote $g(\tau)$ as the amount of energy purchased from the power grid, which is upper bounded by $g_{\max}$ at slot τ.

Remark 2: Notably, the EH process and electricity price vary much slower than data arrival and channel fading. The latter two change at every data slot, while the former two change at every energy frame, i.e., every T data slots. On the other hand, in order to accomplish stable power supply, the grid energy is expected as a supplement of the clean energy. As a result, the BS has to schedule $\vartheta(\tau)$ and $g(\tau)$ on the same time scale.

Denote $p_c(\tau)$ as the total amount of energy consumed by the BS at data slot τ, which is given by

$$p_c(\tau) = \sum_{n=1}^{N} \sum_{k=1}^{K} x_{n,k}(\tau)\, p_{n,k}(\tau) T_0 \tag{8}$$

The battery state of the BS can be regarded as an energy queue, where the harvested and purchased energy serves as energy input, and the consumed energy serves as energy output. The energy queue backlog $E(\tau)$ is evolved as

$$E(\tau+1) = \max\left[E(\tau) - p_c(\tau), 0\right] + g(\tau) + \vartheta(\tau) \tag{9}$$

According to the causality constraint, the consumed energy is bounded by $p_c(\tau) \leq E(\tau)$, which means that the consumed energy cannot exceed the currently available energy in the battery. On the other hand, the energy queue backlog is also limited by the battery capacity E_{max}, i.e.,

$$E(\tau) + g(\tau) + \vartheta(\tau) \leq E_{\max} \tag{10}$$

III. Problem Formulation

In this paper, we aim at maximizing the long-term QoE performance of the overall network while minimizing the energy cost. The objective function is defined as a weighted sum of QoE and energy cost, which is given by

$$f(\tau) = \sum_{n=1}^{N} U_n(\tau) - \beta \eta(\tau) g(\tau) \tag{11}$$

where $\eta(\tau)$ is the electricity price of grid power, which also changes every energy frame. To encourage the consumption of harvested energy, the price of harvested energy is set as zero. β is a parameter used to balance the tradeoff between energy cost and QoE.

Denote $\mathbf{r}(\tau) = \{r_n(\tau)\}$, $\mathbf{x}(\tau) = \{x_{n,k}(\tau)\}$, and $\mathbf{p}(\tau) = \{p_{n,k}(\tau)\}$ as the sets of rate control, channel selection, and power allocation optimization variables, respectively. The two-timescale resource allocation problem with long-term optimization objective is formulated as

$$\begin{aligned}
\mathbf{P1}: \quad & \underset{g(\tau), \vartheta(\tau), \mathbf{r}(\tau), \mathbf{x}(\tau), \mathbf{p}(\tau)}{\text{maximize}} \quad \lim_{M\to\infty} \frac{1}{MT} \sum_{\tau=1}^{MT} f(\tau) \\
& \text{s.t.} \\
& \mathrm{C}_1: 0 \le \vartheta(\tau) \le \Phi(\tau), \forall \tau \\
& \mathrm{C}_2: 0 \le g(\tau) \le g_{\max}, \forall \tau \\
& \mathrm{C}_3: 0 \le E(\tau) + g(\tau) + \vartheta(\tau) \le E_{\max}, \forall \tau \\
& \mathrm{C}_4: 0 \le p_c(\tau) \le E(\tau), \forall \tau \\
& \mathrm{C}_5: 0 \le p_{n,k}(\tau) \le p_{n,k}^{\max}, \forall k, \forall n, \forall \tau \\
& \mathrm{C}_6: x_{n,k}(\tau) \in \{0,1\}, \forall k, \forall n, \forall \tau, \\
& \mathrm{C}_7: \sum_{k=1}^{K} x_{n,k}(\tau) \le q, \forall n, \forall \tau \\
& \mathrm{C}_8: \sum_{n=1}^{N} x_{n,k}(\tau) \le 1, \forall k, \forall \tau \\
& \mathrm{C}_9: 0 \le \sum_{n=1}^{N} r_n(\tau) \le R_{max}, \forall \tau \\
& \mathrm{C}_{10}: d_n \le d_n^*, \forall n \\
& \mathrm{C}_{11}: E,\ Q_n, \forall n, \text{ are mean rate stable.}
\end{aligned} \tag{12}$$

Here, C_1 and C_2 denote the upper bounds of harvested energy and purchased energy, respectively. C_3 is the battery capacity constraint. C_4 is the energy causality constraint. C_5 is the instantaneous constraint of maximum transmission power. $\mathrm{C}_6 - \mathrm{C}_8$ denote the channel selection constraints,

i.e., each channel could be only used by one device and one device could use at most q channels. q also indicates the quota of channel for device, i.e., the maximum number of channels that can be allocated to any device. C_9 is the instantaneous rate control constraint of the overall network. C_{10} is the time-average delay constraint. C_{11} denotes the stability constraints of data queue and energy queue.

There are several key challenges that have to be addressed when solving problem $\mathbf{P1}$. First, $\mathbf{P1}$ involves the joint optimization of rate control, channel selection, power allocation, and energy management from a long-term perspective under both long-term and short-term constraints. However, the prior knowledge of future CSI, data arrival, energy arrival and electricity price is unknown. Second, it involves resource allocation with different timescales, i.e., rate control, channel selection, and power allocation have to be jointly optimized every data slot, while energy management has to be optimized every energy frame. Third, it is an mixed integer nonlinear optimization (MINP) problem which involves both binary and continuous optimization variables. Last but not least, the sum-rate constraint C_9 raises scalability issues for real-world implementation as the problem dimension increases significantly with the number of IIoT devices. Therefore, how to solve $\mathbf{P1}$ remains nontrivial.

IV. Two-Timescale Resource Allocation Optimization

In this section, we aim to solve the two-timescale long-term optimization problem, by combining Lyapunov optimization, ADMM and matching theory. First, Lyapunov optimization is introduced to transform the long-term optimization problem into a series of single-slot optimization subproblems, which are further decomposed over two timescales. Then, ADMM is introduced to solve the large-scale rate control problem with the sum-rate constraint. Finally, a joint channel selection and power allocation algorithm is developed based on price-based one-to-many matching. The proposed two-timescale resource allocation algorithm is summarized in Algorithm 1.

A. Problem Transformation and Decomposition based on Lyapunov Optimization

Denote $\mathcal{Q}(\tau) = [Q_1(\tau), Q_2(\tau), \cdots, Q_N(\tau)]$. Let $\mathcal{H}(\tau) = [\mathcal{Q}(\tau), E(\tau)]$ be a concatenated vector of queue states. Subsequently, the Lyapunov function is defined as [8]

$$L(\tau) = \frac{1}{2}\left\{\sum_{n=1}^{N} Q_n^2(\tau) + [E_{\max} - E(\tau)]^2\right\} \tag{13}$$

Algorithm 1 Two-timescale Resource Allocation Algorithm

Input: N, K, T, M, $E_{\max}$, $g_{\max}$, $p_{n,k}^{\max}$, $R_{\max}$, q.

Output: $\mathbf{g}^*$, $\boldsymbol{\vartheta}^*$, $\mathbf{r}^*$, $\mathbf{x}^*$, $\mathbf{p}^*$.

Initialize: $Q_n(1)$, $E(1)$.

for $m = 1 : M$ **do**

  Energy management: Obtain the optimal solution $g^*[(m-1)T+1]$ and $\vartheta^*[(m-1)T+1]$.

  for $t = 1 : T$ **do**

    Rate control: Obtain the optimal solution $r_n^*[(m-1)T+t], \forall n \in \mathcal{N}$, using Algorithm 2.

    Joint channel selection and power allocation: Obtain the optimal solution $x_{n,k}^*[(m-1)T+t]$ and $p_{n,k}^*[(m-1)T+t]$, $\forall n \in \mathcal{N}, \forall k \in \mathcal{K}$, using price-based one-to-many matching algorithm.

    Update the data queues and the energy queue:

$$\begin{aligned} Q_n[(m-1)T+t+1] = \max\{&Q_n[(m-1)T+t] - v_n[(m-1)T+t]T_0, 0\} \\ &+ r_n[(m-1)T+t]T_0 \\ E[(m-1)+t+1] = \max\{&E[(m-1)+t] - p_c[(m-1)T+t], 0\} \\ &+ g[(m-1)T+t] + \vartheta[(m-1)T+t] \end{aligned}$$

  end for

end for

The Lyapunov drift over T slots which is conditioned on the states of both data queues and energy queue is given by

$$\Delta_T(\tau) = \mathbb{E}[L(\tau+T) - L(\tau) | \mathcal{H}(\tau)] \tag{14}$$

Accordingly, the drift-minus-utility (DMU) function is defined as

$$D[\mathcal{H}(\tau)] = \mathbb{E}[\Delta_T(\tau) - Vf(\tau) | \mathcal{H}(\tau)] \tag{15}$$

where V is a tunable weight which represents the relative importance of "utility maximization" compared with "queue stability".

Considering the timescale difference of energy management, rate control, channel selection, and power allocation, the upper bound of $D\left[\mathcal{H}\left(\tau\right)\right]$ is derived based on the following theorem.

Theorem 1. *The DMU function* $D\left[\mathcal{H}\left(\tau\right)\right]$ *is upper bounded by*

$$\begin{aligned} D\left[\mathcal{H}\left(\tau\right)\right] \leq & \frac{1}{2}\left[B+\frac{\left(T-1\right)}{2}\left(g_{\max}+\vartheta_{\max}\right)^{2}\right]T \\ & +\mathbb{E}\left\{D_{1}\left[\left(m-1\right)T+1\right]+\sum_{\tau=(m-1)T+1}^{mT}\left[D_{2}\left(\tau\right)-D_{3}\left(\tau\right)\right]\right\} \end{aligned} \tag{16}$$

where

$$\begin{aligned} B= & N\left(r_{\max}^{2}+v_{\max}^{2}\right)T_{0}^{2}+E_{\max}^{2}+\left(g_{\max}+\vartheta_{\max}\right)^{2} \\ \mathcal{E}\left[\left(m-1\right)T+1\right]= & E_{\max}-E\left[\left(m-1\right)T+1\right] \\ D_{1}\left[\left(m-1\right)T+1\right]= & \left\{VT\beta\eta\left[\left(m-1\right)T+1\right]-\mathcal{E}\left[\left(m-1\right)T+1\right]\right\}g\left[\left(m-1\right)T+1\right] \\ & -\mathcal{E}\left[\left(m-1\right)T+1\right]\vartheta\left[\left(m-1\right)T+1\right] \\ D_{2}\left(\tau\right)= & \sum_{n=1}^{N}\left[Q_{n}\left(\tau\right)r_{n}\left(\tau\right)T_{0}-VU_{n}\left(\tau\right)\right] \\ D_{3}\left(\tau\right)= & \sum_{n=1}^{N}\sum_{k=1}^{K}x_{n,k}\left(\tau\right)\left[Q_{n}\left(\tau\right)v_{n}\left(\tau\right)T_{0}-\mathcal{E}\left(\tau\right)p_{n,k}\left(\tau\right)\right] \end{aligned}$$

Proof: See Appendix A. ■

In the Theorem 1, B is a positive constant. Following the Lyapunov optimization approach, the problem (12) could be transformed into opportunistically minimizing the right-hand side of (16) at each energy frame subject to $\mathrm{C}_{1}\sim\mathrm{C}_{10}$. Thus, the long-term stochastic optimization problem $\mathbf{P1}$ is converted into a deterministic short-term optimization problem, which is given by

$$\begin{aligned} \mathbf{P2}: & \underset{g[(m-1)T+1],\vartheta[(m-1)T+1],\mathbf{r}(\tau),\mathbf{x}(\tau),\mathbf{p}(\tau)}{\text{minimize}} D_{1}\left[\left(m-1\right)T+1\right]+\sum_{\tau=(m-1)T+1}^{mT}\left[D_{2}\left(\tau\right)-D_{3}\left(\tau\right)\right] \\ & \text{s.t. } \mathrm{C}_{1}-\mathrm{C}_{10} \end{aligned} \tag{17}$$

It is noted that the first term of $\mathbf{P2}$ involves only the energy management decisions $g\left[\left(m-1\right)T+1\right]$, and $\vartheta\left[\left(m-1\right)T+1\right]$, the second term involves only the rate control decisions $\mathbf{r}\left(\tau\right)$, and the third term involves only the joint channel selection and power allocation decisions $\mathbf{x}\left(\tau\right)$, and

$\mathbf{p}(\tau)$. Therefore, we can further decompose $\mathbf{P2}$ into three subproblems with different timescales, which are introduced as follows.

1) Energy management at each energy frame: Both electricity price and energy arrival change every T slots. Accordingly, BS schedules the harvested energy and the purchased energy every T data slots. To minimize the first term $D_1[(m-1)T+1]$, $\forall m \in \{1,2,\ldots,M\}$ the following energy management subproblem is solved at $\tau=(m-1)T+1$, which is given by

$$\begin{aligned}\mathbf{P3}: &\underset{g[(m-1)T+1],\vartheta[(m-1)T+1]}{\text{minimize}} D_1[(m-1)T+1]\\ &\text{s.t. } \mathrm{C}_1, \mathrm{C}_2, \mathrm{C}_3, \tau=(m-1)T+1\end{aligned} \tag{18}$$

Minimizing $D_1[(m-1)T+1]$ is equivalent to using harvested energy as much as possible. However, the available amount of harvested energy is limited by the upper bounds of both the harvested energy $\Phi[(m-1)T+1]$ and the remaining battery capacity $\mathcal{E}[(m-1)T+1]$. Therefore, the optimal scheduling policy of harvested energy is derived as

$$\vartheta^*[(m-1)T+1]=\min\{\Phi[(m-1)T+1],\mathcal{E}[(m-1)T+1]\} \tag{19}$$

Take $\vartheta^*[(m-1)T+1]$ into $D_1[(m-1)T+1]$ and optimize it, regarding $g[(m-1)T+1]$ under the constraint g_{max}, the optimal amount of purchased energy is derived as

$$\begin{aligned}&g^*[(m-1)T+1]\\ &=\begin{cases}\min\{\mathcal{E}[(m-1)T+1]-\vartheta^*[(m-1)T+1], g_{\max}\}, & \text{if}\,\Psi[(m-1)T+1]<0\\ 0 & \text{otherwise}\end{cases}\end{aligned} \tag{20}$$

where $\Psi[(m-1)T+1]=VT\beta\eta[(m-1)T+1]-\mathcal{E}[(m-1)T+1]$. We could find that the values of $\vartheta[(m-1)T+1]$ and $g[(m-1)T+1]$ are optimized every energy frame, i.e., T data slots, while the energy queue length $E(\tau)$ changes over each data slot. Therefore, the energy scheduling policy only depends on the current energy queue state.

2) Rate control at each data slot: To minimize the second term $D_2(\tau)$, the following rate control subproblem is solved at $\tau \in [(m-1)T+1, mT]$, $\forall m \in \{1,2,\ldots,M\}$ which is given by

$$\begin{aligned}\mathbf{P4}: &\underset{\mathbf{r}(\tau)}{\text{minimize}}\, D_2(\tau)\\ &\text{s.t. } \mathrm{C}_9\end{aligned} \tag{21}$$

$\mathbf{P4}$ can be proved as a convex optimization problem by verifying its corresponding second-order derivative. However, due to the sum-rate constraint C_9, the optimization variables of different devices are coupled with each other, and the computational complexity grows enormously as the

number of devices increases. When the number of IIoT devices is large, it will take tremendous amount of time to solve the large-scale rate control problem by using the conventional convex optimization approach. Thus, we develop a low-complexity rate control algorithm to solve $\mathbf{P4}$ based on ADMM. The details are given in Subsection IV-B.

3) Joint channel selection and power allocation at each data slot: To maximize the third term $D_3(\tau)$, the following joint channel selection and power allocation subproblem is solved at $\tau \in [(m-1)T+1, mT]$, $\forall m \in \{1, 2, \ldots, M\}$ which is given by

$$\begin{aligned} \mathbf{P5}: & \underset{\mathbf{x}(\tau),\mathbf{p}(\tau)}{\text{maximize}}\, D_3(\tau) \\ & \text{s.t. } \mathrm{C}_4 - \mathrm{C}_8, \mathrm{C}_{10} \end{aligned} \tag{22}$$

In $\mathbf{P5}$, the time-average delay constraint C_{10} imposes a new challenge. The tight coupling between $r_n(\tau)$ and $v_n(\tau)$ makes it difficult to transform C_{10} into a constraint of virtual queue stability as [25], [26]. Furthermore, despite the time-average delay constraint, IIoT services and applications also demand strict instantaneous delay constraint. Thus, we tighten the delay constraints over every data slot as

$$\frac{r_n(\tau)}{v_n(\tau)\left[v_n(\tau) - r_n(\tau)\right]} \leq d_n^* \tag{23}$$

Rearranging (23), we can get

$$f_d\left[v_n(\tau)\right] = r_n(\tau) - d_n^*\left[v_n(\tau)\right]^2 + d_n^* v_n(\tau) r_n(\tau) \leq 0 \tag{24}$$

where $f_d\left[v_n(\tau)\right]$ is a one-variable quadratic inequality with respect to $v_n(\tau)$. Since $f_d(0) = r_n(\tau) > 0$ and $d_n^* > 0$, there exist a positive solution and a negative solution which make the equality in (24) hold. The positive solution is given by

$$v_n^*(\tau) = \frac{d_n^* r_n(\tau) + \sqrt{\left[d_n^* r_n(\tau)\right]^2 + 4 r_n(\tau) d_n^*}}{2 d_n^*} \tag{25}$$

Accordingly, the delay constraint could be converted into a transmission capacity constraint as

$$\mathrm{C}_{12}: v_n(\tau) \geq v_n^*(\tau) \tag{26}$$

Replacing C_{10} with C_{12}, $\mathbf{P5}$ is rewritten as

$$\begin{aligned} \mathbf{P6}: & \underset{\mathbf{x}(\tau),\mathbf{p}(\tau)}{\text{maximize}}\, D_3(\tau) \\ & \text{s.t. } \mathrm{C}_4 - \mathrm{C}_8, \mathrm{C}_{12} \end{aligned} \tag{27}$$

How to solve $\mathbf{P6}$ is provided in Subsection IV-C.

B. Low-complexity Rate Control Algorithm based on ADMM

ADMM provides a powerful methodology to solve large-scale high-dimensional data processing and control optimization problems. It has already been successfully applied in various aspects including distributed energy management, machine learning, and image recognition [27]. The major concept of ADMM is to alternatively update primal and dual variables in an iterative fashion [28]. It can rapidly find the optimal solution in low complexity based on the decomposition-coordination approach.

In order to obtain the optimal solution, we partition the vector of rate control variables into two parts, i.e., $\mathbf{r_1} = [r_1(\tau), r_2(\tau), \cdots, r_{l_r}(\tau)]$ and $\mathbf{r_2} = [r_{l_r+1}(\tau), r_{l_r+2}(\tau), \cdots, r_N(\tau)]$. Then defining $\mathbf{x}_r = \mathbf{r_1}^T$ and $\mathbf{z}_r = \mathbf{r_2}^T$, $\mathbf{P4}$ is rewritten as [29]

$$\begin{aligned} &\mathbf{P7}: \underset{\mathbf{x}_r, \mathbf{z}_r}{\text{minimize}}\, F_r(\mathbf{x}_r) + G_r(\mathbf{z}_r) \\ &\text{s.t. } \mathbf{A}_r\mathbf{x}_r + \mathbf{B}_r\mathbf{z}_r = C_r \end{aligned} \tag{28}$$

where $\mathbf{x}_r \in \mathbb{R}^{l_r \times 1}$, $\mathbf{z}_r \in \mathbb{R}^{(N-l_r)\times 1}$, $\mathbf{A}_r \in \mathbb{R}^{1\times l_r}$, $\mathbf{B}_r \in \mathbb{R}^{1\times(N-l_r)}$, and $C_r = R_{max}$. $\mathbf{A}_r$ and $\mathbf{B}_r$ are unit vectors. $F_r(\mathbf{x}_r)$ and $G_r(\mathbf{z}_r)$ satisfy

$$F_r(\mathbf{x}_r) = \mathbf{Q}_1\mathbf{x}_r - \mathbf{V}_{1,\chi}\log_2(\mathbf{x}_r) \tag{29}$$

$$G_r(\mathbf{z}_r) = \mathbf{Q}_2\mathbf{z}_r - \mathbf{V}_{2,\chi}\log_2(\mathbf{z}_r) \tag{30}$$

where $\mathbf{Q}_1 = [Q_1(\tau), Q_2(\tau), \cdots, Q_{l_r}(\tau)]\, T_0$, $\mathbf{Q}_2 = [Q_{l_r+1}(\tau), Q_{l_r+2}(\tau), \cdots, Q_N(\tau)]\, T_0$, $\mathbf{V}_{1,\chi} = [\chi_1, \chi_2, \cdots, \chi_{l_r}]\, V$, and $\mathbf{V}_{2,\chi} = [\chi_{l_r+1}, \chi_{l_r+2}, \cdots, \chi_N]\, V$.

In this paper, we adopt the scaled ADMM algorithm [27], and form the augmented Lagrangian associated with $\mathbf{P7}$ as

$$\mathbf{L}_\rho(\mathbf{x}_r, \mathbf{z}_r, y) = F_r(\mathbf{x}_r) + G_r(\mathbf{z}_r) + \frac{\rho}{2}\|R + \mu\|_2^2 - \frac{\rho}{2}\|\mu\|_2^2 \tag{31}$$

where $R = \mathbf{A}\mathbf{x}_r + \mathbf{B}\mathbf{z}_r - C_r$ is the residual. $\rho > 0$ represents the penalty parameter, which is related to the convergence speed of ADMM. Let y be the Lagrange multiplier. $\mu = \dfrac{y}{\rho}$ is the scaled dual variables. Then, we can iteratively update both primal and dual variables as

$$\mathbf{x}_r^{i+1} = \arg\min\left\{F_r\left(\mathbf{x}_r^i\right) + \frac{\rho}{2}\left\|\mathbf{A}_r\mathbf{x}_r^i + \mathbf{B}_r\mathbf{z}_r^i - C_r + \mu^i\right\|_2^2\right\} \tag{32}$$

$$\mathbf{z}_r^{i+1} = \arg\min\left\{G_r\left(\mathbf{z}_r^i\right) + \frac{\rho}{2}\left\|\mathbf{A}_r\mathbf{x}_r^{i+1} + \mathbf{B}_r\mathbf{z}_r^i - C_r + \mu^i\right\|_2^2\right\} \tag{33}$$

$$\mu^{i+1} = \mu^i + \mathbf{A}_r\mathbf{x}_r^{i+1} + \mathbf{B}_r\mathbf{z}_r^{i+1} - C_r \tag{34}$$

where i denotes the index of iteration.

Algorithm 2 ADMM-based Low-complexity Rate Control Algorithm

1: **Initialize:** i, $\mathbf{x}_r$, $\mathbf{z}_r$,μ ,ρ, ϵ^{pri}, and ϵ^{dual}.
2: **output:** $\mathbf{x}_r$, $\mathbf{z}_r$.
3: **while** $\left\|\mathbf{R_p}^i\right\|_2 > \epsilon^{pri}$ or $\left\|\mathbf{R_d}^i\right\|_2 > \epsilon^{dual}$ **do**
4: Update $\mathbf{x}_r^{i+1}$ according to (32);
5: Update $\mathbf{z}_r^{i+1}$ according to (33);
6: Update μ^{i+1} according to (34);
7: Update $\left\|\mathbf{R_p}^{i+1}\right\|_2$ and $\left\|\mathbf{R_d}^{i+1}\right\|_2$;
8: Update $i \to i+1$;
9: **end while**

Next, based on the optimality conditions [30], the primal residual $\mathbf{R_p}$ and the dual residual $\mathbf{R_d}$ are expressed as

$$\mathbf{R_p}^{i+1} = \mathbf{A}_r \mathbf{x}_r^{i+1} + \mathbf{B}_r \mathbf{z}_r^{i+1} - C_r \tag{35}$$

$$\mathbf{R_d}^{i+1} = \rho \mathbf{A}_r^T \mathbf{B}_r \left(\mathbf{z}_r^{i+1} - \mathbf{z}_r^i\right) \tag{36}$$

The termination criteria is defined as

$$\left\|\mathbf{R_p}^{i+1}\right\|_2 \leq \epsilon^{pri} \text{ and } \left\|\mathbf{R_d}^{i+1}\right\|_2 \leq \epsilon^{dual} \tag{37}$$

where $\epsilon^{pri} > 0$ and $\epsilon^{dual} > 0$ denote feasibility tolerances with respect to primal conditions and dual conditions. Consequently, the ADMM-based low-complexity rate control algorithm is summarized in Algorithm 2.

C. Joint Channel Selection and Power Allocation based on One-to-many Matching

We rearrange $\mathbf{P6}$ as

$$\begin{aligned} &\underset{\mathbf{x}(\tau),\mathbf{p}(\tau)}{\text{maximize}} \sum_{n=1}^{N} f_{D_3}\left[x_{n,k}\left(\tau\right), p_{n,k}\left(\tau\right)\right] \\ &\text{s.t. } \mathrm{C}_4 - \mathrm{C}_8, \mathrm{C}_{12} \end{aligned} \tag{38}$$

where $f_{D_3}\left[x_{n,k}\left(\tau\right), p_{n,k}\left(\tau\right)\right] = Q_n\left(\tau\right) v_n\left[x_{n,k}\left(\tau\right), p_{n,k}\left(\tau\right)\right] T_0 - \mathcal{E}\left(\tau\right) x_{n,k}\left(\tau\right) p_{n,k}\left(\tau\right)$. The problem defined in (38) is NP-hard due to the coupling between integer variables and continuous variables. To provide a tractable solution, we transfer it into a one-to-many matching problem,

which is represented as a triple $(\mathcal{N}, \mathcal{K}, \mathcal{F})$. $\mathcal{F}$ denotes the set of devices' preference lists. The definition of one-to-many matching is introduced as follows.

Definition 1. ***(One-to-many matching)*** *For the formulated matching problem $\mathcal{M}_{\mathbf{q}} = (\mathcal{N}, \mathcal{K}, \mathcal{F})$, the matching φ is a one-to-many mapping from set $\mathcal{N} \cup \mathcal{K}$ onto itself under preference $\mathcal{F}$, i.e., $\varphi(n) \in \mathcal{K} \cup \{n\}$, $\forall n \in \mathcal{N}$. $\varphi(n) = k$ means that channel k is matched with device n, i.e., $x_{n,k} = 1$. $\varphi(n) = n$ represents that device n is not matched with any channel. Quota is set as $\mathbf{q} = [q, 1]$, i.e., each device could select at most q channels and each channel could be only used by at most one device.*

A matching φ is blocked if device n and channel k are not matched with each other but prefer each other to their mates under φ. Thus, n and k form a blocking pair for matching φ, namely that (n, k) blocks the matching. We say that matching φ is not stable because n and k would prefer to disrupt the matching in order to be matched with each other.

Definition 2. ***(Stable matching)*** *A matching φ is stable if there exists no blocking pair.*

When $\varphi(n) = k$, the maximum value of $f_{D_3}\left[p_{n,k}(\tau) | x_{n,k}(\tau) = 1\right]$ can be obtained by solving the following power allocation problem

$$\begin{aligned} &\mathbf{P8}: \underset{p_{n,k}(\tau)}{\text{maximize}}\, f_{D_3}\left[p_{n,k}(\tau) | x_{n,k}(\tau) = 1\right] \\ &\text{s.t. } \mathrm{C}_5 \end{aligned} \tag{39}$$

$\mathbf{P8}$ is also a convex optimization problem and can be solved by applying Karush-Kuhn-Tucker (KKT) conditions. The Lagrangian associated with $\mathbf{P8}$ is given by

$$\mathcal{L}\left[p_{n,k}(\tau), \lambda\right] = -f_{D_3}\left[p_{n,k}(\tau) | x_{n,k}(\tau) = 1\right] + \lambda\left[p_{n,k}(\tau) - p_{n,k}^{\max}\right] \tag{40}$$

where λ is the Lagrange multiplier corresponding to constraint C_5. The optimal solution $p_{n,k}^*(\tau)$ is given by

$$p_{n,k}^*(\tau) = \min\left[p_{n,k}^{\max}, \frac{Q_n(\tau) T_0 B_k(\tau)}{\mathcal{E}(\tau) \ln 2} - \frac{\sigma^2}{h_{n,k}(\tau)}\right] \tag{41}$$

We can notice that $p_{n,k}^*(\tau)$ is positively related to $Q_n(\tau)$, and is negatively related to $h_{n,k}(\tau)$ and $\mathcal{E}(\tau)$.

We define the preference of device n towards channel k as

$$F_{n,k}|_{\varphi(n)=k} = f_{D_3}\left[p_{n,k}^*(\tau) | x_{n,k}(\tau) = 1\right] - \Lambda_k \tag{42}$$

where Λ_k is the virtual price of channel k which is added to resolve the conflict of matching. It can be set as zero initially.

Thus, by temporarily matching device n with every channel, we can obtain its preferences towards all the channels. The preference list of device n, i.e., $\mathcal{F}_n$, is constructed by sorting all K channels in descending order according to the preferences, i.e., $F_{n,k}|_{\varphi(n)=k}$, $\forall k \in \mathcal{K}$. The total set $\mathcal{F}$ is constructed as $\mathcal{F} = \{\mathcal{F}_n, \forall n \in \mathcal{N}\}$. Then, the price-based one-to-many matching is implemented as follows.

Initially, set $\varphi(n) = \emptyset$, $\Omega = \emptyset$, and $\Lambda_k = 0$, $\forall k \in \mathcal{K}$. Ω represents the set of channels which receive more than one matching proposal from devices.

In the proposal process, if $\exists \varphi(n) = \emptyset$, device $n \in \mathcal{N}$ will propose to the first q channels in its preference list $\mathcal{F}_n$. Afterwards, if any channel $k \in \mathcal{K}$ receives only one proposal from a device, then they will be directly matched. Otherwise, if k receives more than one proposal, add k into set Ω and enter into the price rising process.

In the price rising process, every channel $k \in \Omega$ increases its price Λ_k by $\Delta\Lambda_k$. Accordingly, all the devices that are competing for channel k have to update their preferences towards channel k and renew their proposals. A device may give up channel k if its price is too high. The price rising process will continue until only one device remains, which is eventually matched with channel k, Then, k is removed from Ω.

The iterative matching process will be finished until a stable matching is produced.

V. Performance analysis

In this section, some theoretical properties in terms of optimality performance, convergence performance, and computational complexity are analyzed.

A. Trade-off between Queue Stability and Utility Maximization

Theorem 2. *Algorithm 1 achieves a* $\left[O(V), O\left(1/V\right)\right]$ *trade-off between queue stability and utility maximization by adjusting the control parameter* V*. The time-average data queue backlog,*

time-average energy queue backlog, and time-average network utility are bounded by

$$\lim_{M\to\infty}\frac{1}{MT}\mathbb{E}\left[\sum_{m=1}^{M}\sum_{\tau=(m-1)T+1}^{mT}\sum_{n=1}^{N}Q_n\left(\tau\right)\right]\leq\frac{B}{2\delta_1}+\frac{V\left(f_{\max}-f_{opt}\right)}{\delta_1} \tag{43}$$

$$\lim_{M\to\infty}\frac{1}{MT}\mathbb{E}\left[\sum_{m=1}^{M}\sum_{\tau=(m-1)T+1}^{mT}E\left(\tau\right)\right]\geq E_{max}-\frac{B}{2\delta_2}-\frac{V\left(f_{\max}-f_{opt}\right)}{\delta_2} \tag{44}$$

$$\lim_{M\to\infty}\frac{1}{MT}\mathbb{E}\left[\sum_{m=1}^{M}\sum_{\tau=(m-1)T+1}^{mT}f\left(\tau\right)\right]\geq f_{opt}-\frac{B}{2V} \tag{45}$$

Proof: See Appendix B. ■

Theorem 3. *The joint channel selection and power allocation algorithm produces a stable matching between devices and channels within finite iterations, which is also weak-Pareto optimal for devices.*

Proof: Due to the space limitation, the detailed proof is omitted here. A similar proof can be found in [31], [32]. ■

B. Convergence of ADMM-based Low-complexity Rate Control Algorithm

The objective function of $\mathbf{P7}$ is closed, proper, and convex, and the Lagrangian $\mathbf{L}_\rho(\mathbf{x}_r,\mathbf{y}_r,\mathbf{y})$ has a saddle point. Thus the iterations satisfy the following convergence properties.

Theorem 4. *The residual convergence, objective convergence, and dual variable convergence are expressed as follows:*

1) *Residual convergence: The primal and dual residuals converge to 0 as $i\to\infty$, which implies that the iterations approach feasibility.*
2) *Objective convergence: The objective function of $\mathbf{P7}$ eventually converges to the primal optimal value under the stopping criterion as $i\to\infty$.*
3) *Dual variable convergence: The dual variable y^{i+1} eventually converges to the dual optimal value under the stopping criterion as $i\to\infty$.*

Proof: Due to the space limitation, the detailed proof is omitted here. A similar proof can be found in [33]. ■

TABLE I

SIMULATION PARAMETERS.

Parameter	**Value**
Number of devices	$N = 5$
Number of channels	$K = 12$
Channel bandwidth	$B = 1$ MHz
Tunable weight of DMU	$V = 100$
Number of energy frames	$M = 200$
Number of data slots at each energy frame	$T = 5$
One data slot duration	$T_0 = 1$ second
Upper bound of purchased energy	$g_{max} = 2.5$ joule(J)
Capacity of recharge battery	$E_{\max} = 5$ J
Maximum sum of arrival data	$R_{\max} = 20$ Mbps
Service weight parameter	$\chi = [0.1, 0.15, 0.2, 0.25, 0.3]$
Penalty factor of utility	$\beta = \{0, 5000\}$
The initial state of data queue	$Q_n(1) = 3$ Mbits
The initial state of energy queue	$E(1) = 2$ J
Time-average delay constraint	$d_n^* = 10$ microseconds
Quota restriction	$\mathbf{q} = [3, 1]$

C. Computational Complexity

1) Computational complexity of energy management: The energy management problem is a linear programming problem with two variables, which are optimized at each energy frame. Thus, its computational complexity of $O(2M)$.

2) Computational complexity of rate control: Rate control is optimized at each data slot with N optimization variables. Thus, updating primal and dual variables introduces a complexity of $O[\max(l_r, N - l_r)]$. Assuming that $\mathbf{x}_r$, $\mathbf{z}_r$, and $\boldsymbol{\mu}$ are updated ξ times before reaching convergence, the total complexity of rate control is $O[\max(l_r, N - l_r) \times MT\xi]$.

3) Computational complexity of joint channel selection and power allocation: The complexities for each device to acquire the preferences and construct the preference list are $O(K)$ and $O(K \log(K))$, respectively. Assuming that the number of iterations required for resolving the conflict in the price rising process is ς, and there are $\max(N, K)$ conflict elements in the price rising process, the complexity is $O\{MT\{\max(N, K) \times \varsigma + [NK + NK \log(K)]\}\}$.

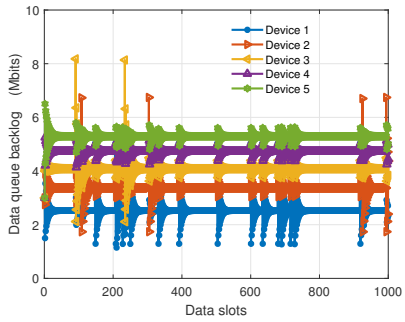


Fig. 2. Data queue backlog of the proposed algorithm.

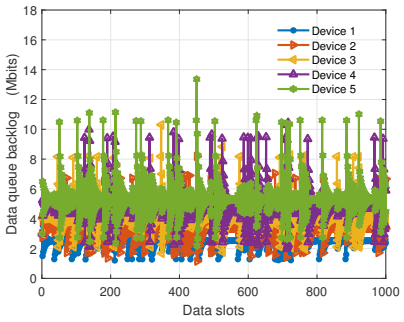


Fig. 3. Data queue backlog of the baseline 1 algorithm.

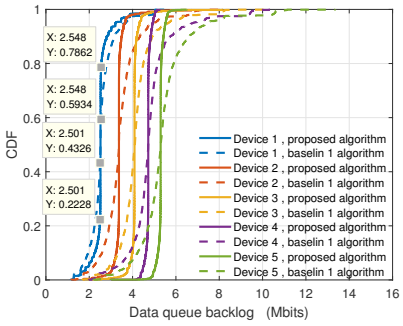


Fig. 4. CDF of data queue backlog.

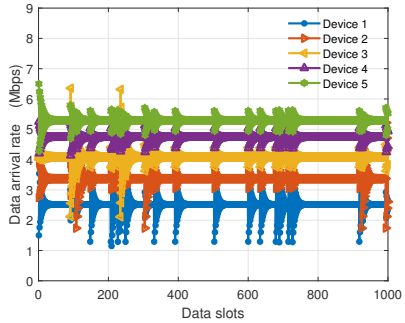


Fig. 5. Data arrival rate of the proposed algorithm.

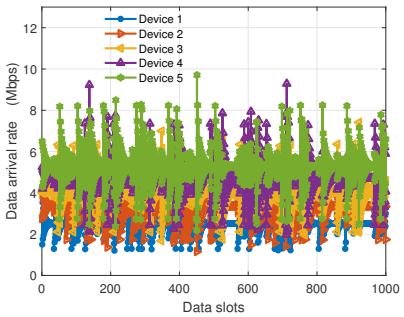


Fig. 6. Data arrival rate of the baseline 1 algorithm.

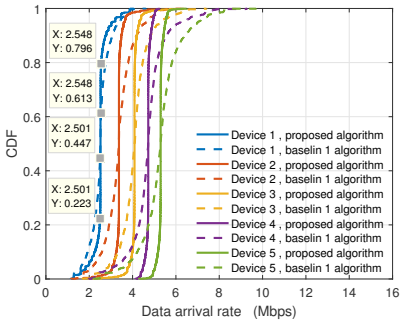


Fig. 7. CDF of data arrival rate.

VI. Simulation Results

In this section, we verify the proposed two-timescale resource allocation algorithm through simulations. Simulation parameters are summarized in Table I [12] [34]. Three heuristic algorithms are used as baseline for comparison purpose. In the baseline 1 algorithm, the optimization of channel selection is neglected, and channels are allocated to devices randomly [32]. The baseline 2 algorithm only maximizes the time-average QoE of network, while the minimization of energy cost is neglected, i.e., $\beta = 0$. In the baseline 3 algorithm, the rate control problem is solved by the convex optimization toolbox [34], i.e., the CVX toolbox.

A. Data Queue Performance

1) Data queue backlog: Fig. 2 and Fig. 3 show the evolutions of data queue backlog corresponding to the proposed algorithm and the baseline 1 algorithm, respectively. It is observed that data queue backlog of the proposed algorithm tends to be stable within a short period of

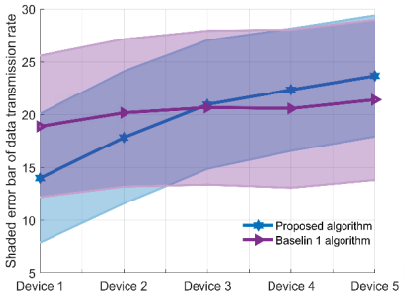


Fig. 8. Shaded error bar of transmission rate.

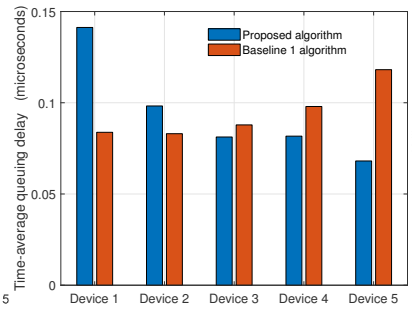


Fig. 9. Time-average queueing delay.

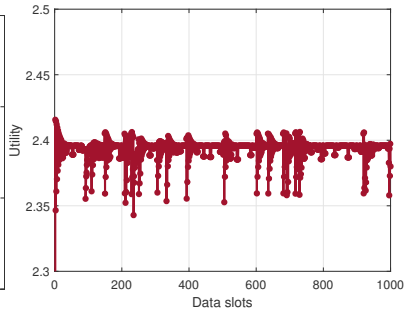


Fig. 10. Network utility of the proposed algorithm.

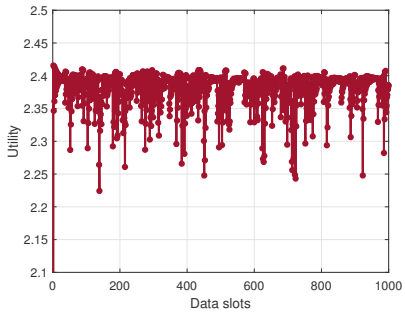


Fig. 11. Network utility of the baseline 1 algorithm.

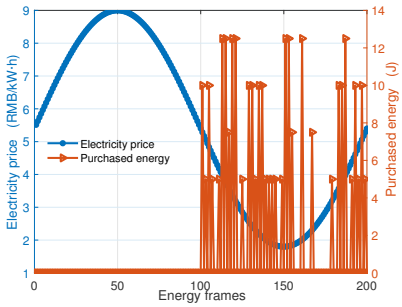


Fig. 12. Grid energy consumption of the proposed algorithm.

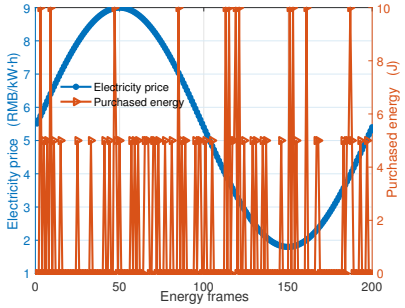


Fig. 13. Grid energy consumption of the baseline 2 algorithm.

time, which guarantees reliable service provision, while the data queue backlog of the baseline 1 algorithm fluctuates more violently, thus making the network less stable. Compared with the baseline 1 algorithm, the proposed algorithm can reduce the peak to average ratio (PAR) of data queue backlog by 35.5%. This phenomenon has also been validated in Fig. 4, which shows the empirical cumulative distribution function (CDF) performance of data queue backlog. Taking device 1 as an example, the probability that the data queue backlog Q_1 lies within the region $[2.501, 2.548]$ is 0.5604, while the probability corresponding to the baseline 1 algorithm is only 0.1608.

2) Data arrival rate: The data arrival rate performances for the proposed algorithm and the baseline 1 algorithm are shown in Fig. 5 to Fig. 7. Similar as in the data queue backlog performance, the data arrival rate fluctuation of the proposed algorithm is much less than that of the baseline 1 algorithm. The proposed algorithm can reduce the PAR of data arrival rate by 28.5%, which infers a more stable rate control performance.

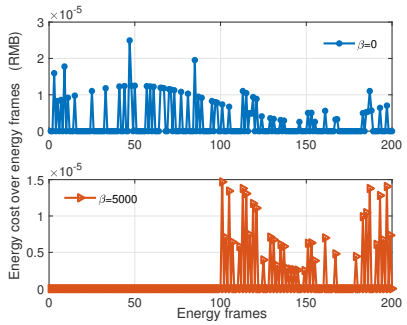


Fig. 14. Energy cost for the proposed algorithm and the baseline 2 algorithm.

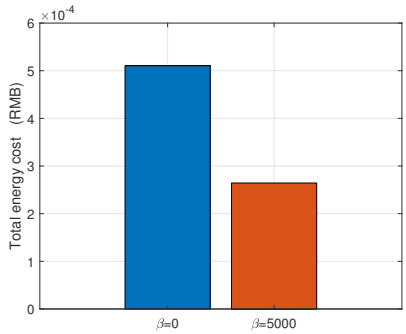


Fig. 15. Total energy cost over 200 energy frames.

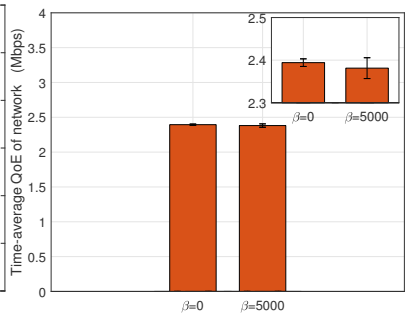


Fig. 16. Time-average QoE of network with standard deviation.

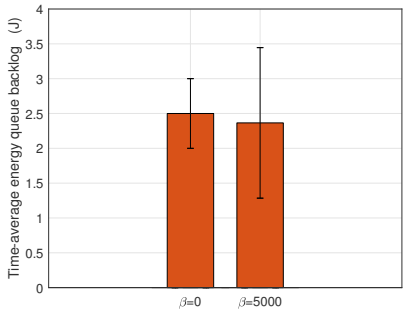


Fig. 17. Time-average energy queue backlog with standard deviation.

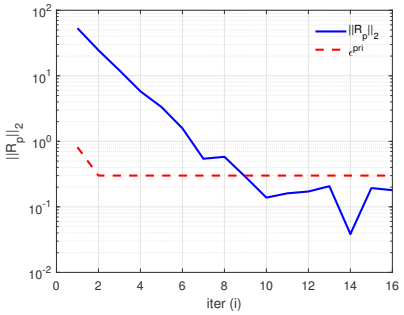


Fig. 18. Convergence of primal variables.

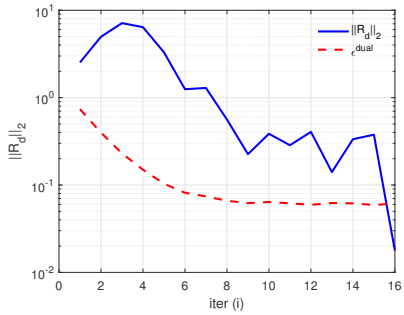


Fig. 19. Convergence of dual variables.

3) Data transmission rate: Fig. 8 shows the shaded error bar of data transmission rate, where the width of the shadow represents the standard deviation. Compared with the baseline 1 algorithm, the proposed algorithm has a much narrower shadow, which provides a more stable transmission rate. Furthermore, we can find that the proposed algorithm can differentiate devices with different service priorities by providing higher transmission rate to devices with larger service weights. In comparison, the baseline 1 algorithm treats all the devices as if they have the same service weight.

4) Queuing delay: Fig. 9 shows the time-average queuing delay performance. For the proposed algorithm, we can find that devices with higher service priorities, e.g., device 5, experience less delay compared with devices with lower service priorities, e.g., device 1. This is consistent with the transmission rate results shown in Fig. 8. While for the baseline 1 algorithm, delay is uncorrelated with service priority, thus making differentiated service provisioning impossible.

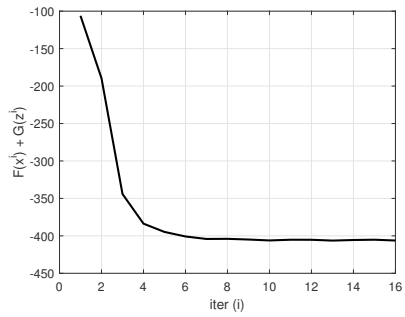


Fig. 20. Convergence of objective value.

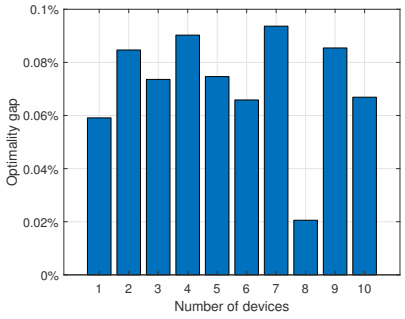


Fig. 21. Optimality gap versus the number of devices.

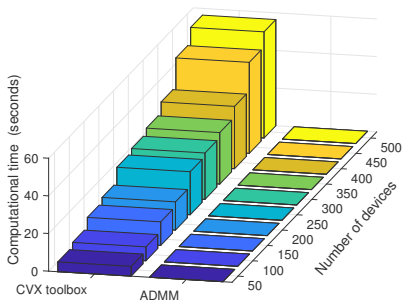


Fig. 22. Computational time versus the number of devices.

5) Network utility: Fig. 10 and Fig. 11 show the network utility performances of the proposed algorithm and the baseline 1 algorithm, respectively. The proposed algorithm achieves more stable network utility performance than the baseline 1 algorithm, which implies a better adaptiveness to the random variation of channel state.

B. Energy Queue Performance

1) Grid energy consumption: Fig. 12 and Fig. 13 show the relations between electricity price and grid energy consumption for the proposed algorithm and the baseline 2 algorithm respectively. We assume that the variation of electricity price follows a sinusoid with the minimum value of 1.8 RMB/kWh and the maximum value of 9.0 RMB/kWh. Simulation results demonstrate that the proposed algorithm can dynamically adapt grid energy consumption with time-varying electricity price by avoiding purchasing the expensive grid power during the peak-price period. In comparison, the baseline 2 algorithm is unaware of the energy cost, and consumes grid energy any time if needed. This inevitably leads to higher energy cost, which is demonstrated in Fig. 14 and Fig. 15.

2) Grid energy cost: Fig. 14 and Fig. 15 show the grid energy cost per energy frame and the total energy cost accumulated over 200 energy frames, respectively. Compared with the baseline 2 algorithm, the proposed algorithm can reduce the energy cost by 48.23%, due to the awareness of electricity price and dynamic adaptation of gird energy consumption.

3) QoE and energy backlog: Fig. 16 and Fig. 17 show the network QoE and energy queue backlog, respectively, where the bar graph represents the time-average value and the error bar represents standard deviation. It is observed that time-average QoE performance of the proposed

algorithm is only 0.54% lower than the baseline 2 algorithm, while the energy queue backlog is only 5.40% lower. In other words, the proposed algorithm trades only 0.54% QoE performance degradation and 5.40% energy queue backlog reduction for energy cost reduction as high as 48.23%.

C. Computational Complexity and Convergence Performances

1) Convergence of Algorithm 2: Fig. 18, Fig. 19, and Fig. 20 show the primal residual converge, dual residual convergence, and optimal convergence of the ADMM-based rate control algorithm at $\tau = 1000$, respectively. It is observed that the stopping criterion constraints ϵ^{pri} and ϵ^{dual}, i.e., the dotted lines shown in Fig. 18 and Fig. 19, can be satisfied within 16 iterations. Fig. 20 demonstrates that the objective value converges to the optimal value within only 7 iterations.

2) Optimality gap and computational complexity: Fig. 21 and Fig. 22 compare optimality and computational complexity between the proposed algorithm and the baseline 3 algorithm, respectively. Simulation results demonstrate that the performance gap between the two algorithms is always less than 1%. On the other hand, the proposed algorithm can reduce the computational time by 99% compared with the baseline 3 algorithm. Furthermore, the computational time of the baseline 3 algorithm increases significantly with the number of devices, while that of the proposed algorithm remains in a much lower level.

VII. Conclusions

In this paper, we studied the two-timescale resource allocation problem in 5G-empowered networks for IIoT applications. We proposed a two-timescale resource allocation algorithm to maximize the long-term QoE performance while simultaneously minimizing the grid energy cost, in which the optimization of energy management is performed every energy frame, while the optimization of rate control, channel selection, and power allocation is performed every data slot. We proved that the proposed algorithm can achieve bounded performance deviation based only on causal information of CSI, EH, and electricity price. We further compare it with three heuristic algorithms under various simulation configurations. Simulation results demonstrate that the proposed algorithm can effectively reduce the PARs of data queue backlog and data arrival rate by 35.5% and 28.5%, respectively. It allows differentiated service provision and achieves 48.23% energy cost reduction by dynamically adapt resource allocation with service priority and time-varying electricity price. It is able to trade only 1% optimality performance degradation for

99% computation time reduction. In the future work, we plan to study how to adopt the machine learning with existing framework to further improve the performance.

APPENDIX A
PROOF OF THEOREM 1

According to (4), for any nonnegative real numbers $Q_n(\tau)$, $r_n(\tau)$ and $v_n(\tau)$, there holds

$$\frac{1}{2}\left[Q_n^2(\tau+1)-Q_n^2(\tau)\right] \leq \frac{1}{2}r_n^2(\tau)T_0^2+\frac{1}{2}v_n^2(\tau)T_0^2+Q_n(\tau)\left[r_n(\tau)-v_n(\tau)\right]T_0 \tag{46}$$

Applying the law of telescoping sums over $\tau \in [(m-1)T+1, mT]$, we can derive

$$\begin{aligned}\frac{1}{2}\left[Q_n^2(\tau+T)-Q_n^2(\tau)\right] \leq & \frac{1}{2}\sum_{\tau=(m-1)T+1}^{mT}\left[r_n^2(\tau)+v_n^2(\tau)\right]T_0^2 \\ & +\sum_{\tau=(m-1)T+1}^{mT}\left\{Q_n(\tau)\left[r_n(\tau)-v_n(\tau)\right]\right\}T_0\end{aligned} \tag{47}$$

Similarly, for energy queue, we can derive

$$\frac{1}{2}\left[\mathcal{E}^2(\tau+1)-\mathcal{E}^2(\tau)\right] \leq \frac{1}{2}p_c^2(\tau)+\left[g(\tau)+\vartheta(\tau)\right]^2+\mathcal{E}(\tau)\left\{p_c(\tau)-\left[g(\tau)+\vartheta(\tau)\right]\right\} \tag{48}$$

Combining (47) and (48) as well as applying the law of telescoping sums and the law of iterated expectations, we derive

$$\begin{aligned}\Delta_T(\tau) \leq & \frac{1}{2}BT+\sum_{\tau=(m-1)T+1}^{mT}\sum_{n=1}^{N}\mathbb{E}\left\{T_0Q_n(\tau)\left[r_n(\tau)-v_n(\tau)\right]|H(\tau)\right\} \\ & +\sum_{\tau=(m-1)T+1}^{mT}\mathbb{E}\left\{\mathcal{E}(\tau)\left\{p_c(\tau)-\left[g(\tau)+\vartheta(\tau)\right]\right\}|H(\tau)\right\}\end{aligned} \tag{49}$$

Based on the definition of DMU given in (15), we can subtract the term $\mathbb{E}\left[Vf(\tau)|H(\tau)\right]$ from both sides of (49), and then apply the law of iterated expectations to derive the upper bond of DMU, which is given by

$$\begin{aligned}D\left[\mathcal{H}(\tau)\right] \leq & \frac{1}{2}BT+\sum_{\tau=(m-1)T+1}^{mT}\mathbb{E}\left\{\left\{V\beta\eta(t)g(t)-\mathcal{E}(\tau)\left[g(\tau)+\vartheta(\tau)\right]\right\}|\mathcal{H}(\tau)\right\} \\ & +\sum_{\tau=(m-1)T+1}^{mT}\sum_{n=1}^{N}\mathbb{E}\left\{\left\{\left[Q_n(\tau)r_n(\tau)T_0\right]-VU_n(\tau)\right\}|\mathcal{H}(\tau)\right\} \\ & -\sum_{\tau=(m-1)T+1}^{mT}\sum_{n=1}^{N}\sum_{k=1}^{K}x_{n,k}\mathbb{E}\left\{\left\{Q_n(\tau)v_n(\tau)T_0-\mathcal{E}(\tau)p_{n,k}(\tau)\right\}|\mathcal{H}(\tau)\right\}\end{aligned} \tag{50}$$

Define $D_0(\tau)$ as

$$D_0(\tau) = \sum_{\tau=(m-1)T+1}^{mT} \mathbb{E}\left\{\left\{V\beta\eta(t)\, g(t) - \mathcal{E}(\tau)\left[g(\tau) + \vartheta(\tau)\right]\right\} | \mathcal{H}(\tau)\right\} \tag{51}$$

According to the energy causality, for $\forall \tau^{'} > \tau$, the following inequality holds

$$E(\tau) - \left(\tau^{'} - \tau\right) p_c \leq E\left(\tau^{'}\right) \leq E(\tau) + \left(\tau^{'} - \tau\right)\left(g_{\max} + \vartheta_{\max}\right) \tag{52}$$

where ϑ_{max} is the upper bound of $\mathbb{E}\left[\vartheta(\tau)|\mathcal{H}(\tau)\right]$.

Using these inequalities (52) over $\tau \in [(m-1)T+1, mT]$, we can derive

$$\begin{aligned} D_0(\tau) \leq & \frac{(T-1)T}{2}\left(g_{\max} + \vartheta_{\max}\right)^2 + TV\beta\eta\left[(m-1)T+1\right] g\left[(m-1)T+1\right] \\ & + \mathcal{E}\left[(m-1)T+1\right]\left\{g\left[(m-1)T+1\right] + \vartheta\left[(m-1)T+1\right]\right\} \end{aligned} \tag{53}$$

By taking (53) into (50), we can derive (16). This completes the proof of Theorem 1.

APPENDIX B
PROOF OF THEOREM 2

To prove Theorem 2, we introduce some significant and practical assumptions, i.e.,

$$\mathbb{E}\left[r_n(\tau) T_0 - v_n(\tau) T_0 | Q_n(\tau)\right] \leq -\delta_1 \tag{54}$$

$$\mathbb{E}\left\{p_c(\tau) - \left[g(\tau) + \vartheta(\tau)\right] | E(\tau)\right\} \leq -\delta_2 \tag{55}$$

where $\delta_1 > 0$ and $\delta_2 > 0$ are the gap between data queue input and output, and the gap between energy queue input and output, respectively.

According to Theorem 1, we can derive

$$\begin{aligned} D\left[\mathcal{H}(\tau)\right] \leq & \frac{1}{2}BT - Vf_{opt} \\ & + \sum_{\tau=(m-1)T+1}^{mT} \sum_{n=1}^{N} \mathbb{E}\left\{Q_n(\tau)\left[r_n(\tau) - v_n(\tau)\right]\right\} \\ & + \sum_{\tau=(m-1)T+1}^{mT} \mathbb{E}\left\{\mathcal{E}(\tau)\left\{p_c(\tau) - \left[g(\tau) + \vartheta(\tau)\right]\right\}\right\} \end{aligned} \tag{56}$$

where f_{opt} is the optimal value obtained by Algorithm 1.

Applying the law of telescoping sums over $\tau \in [1, MT]$ and the law of iterated expectations for the above equation, we derive

$$\mathbb{E}\left[L\left(MT\right)-L\left(1\right)-V\sum_{m=1}^{M}\sum_{\tau=(m-1)T+1}^{mT}f\left(\tau\right)\right]\leq\frac{1}{2}MBT$$
$$-\mathbb{E}\left[\sum_{m=1}^{M}\sum_{\tau=(m-1)T+1}^{mT}\sum_{n=1}^{N}Q_n\left(\tau\right)\delta_1\right]-\mathbb{E}\sum_{m=1}^{M}\sum_{\tau=(m-1)T+1}^{mT}E\left(\tau\right)\delta_2-VMTf_{opt} \tag{57}$$

According to (57), we can derive

$$\mathbb{E}\left[L\left(MT\right)-L\left(1\right)-V\sum_{m=1}^{M}\sum_{\tau=(m-1)T+1}^{mT}f\left(\tau\right)\right]$$
$$\leq\frac{1}{2}MBT-\mathbb{E}\sum_{m=1}^{M}\sum_{\tau=(m-1)T+1}^{mT}\sum_{n=1}^{N}Q_n\left(\tau\right)\delta_1-VMTf_{opt} \tag{58}$$

Rearranging (58), we obtain

$$\mathbb{E}\left[\sum_{m=1}^{M}\sum_{\tau=(m-1)T+1}^{mT}\sum_{n=1}^{N}Q_n\left(\tau\right)\delta_1\right]$$
$$\leq\frac{1}{2}MBT-\mathbb{E}\left[L\left(MT\right)-L\left(1\right)\right]+VMT\left(f_{\max}-f_{opt}\right) \tag{59}$$

where $f_{\max}$ is the maximum value of network utility. There exists a bound that $f_{\max} \geq f_{opt}$.

Dividing both sides of (59) by $MT\delta_1$ and taking the limit $M \to \infty$, we can obtain

$$\lim_{M\to\infty}\frac{1}{MT}\mathbb{E}\left[\sum_{m=1}^{M}\sum_{\tau=(m-1)T+1}^{mT}\sum_{n=1}^{N}Q_n\left(\tau\right)\right]\leq\frac{1}{2\delta_1}B+\frac{V\left(f_{\max}-f_{opt}\right)}{\delta_1} \tag{60}$$

Similarly, based on (57), we can obtain

$$\frac{1}{MT}\mathbb{E}\left[\sum_{m=1}^{M}\sum_{\tau=(m-1)T+1}^{mT}\mathcal{E}\left(\tau\right)\right]\leq\frac{1}{2\delta_2}B-\frac{\mathbb{E}\left[L\left(MT\right)-L\left(1\right)\right]}{MT\delta_2}+\frac{V\left(f_{\max}-f_{opt}\right)}{\delta_2} \tag{61}$$

Taking the limit $M \to \infty$ and using $\lim_{M\to\infty}\frac{\mathbb{E}\left[L\left(MT\right)-L\left(1\right)\right]}{MT\delta_2}=0$, we can derive

$$\lim_{M\to\infty}\frac{1}{MT}\mathbb{E}\sum_{m=1}^{M}\sum_{\tau=(m-1)T+1}^{mT}\mathcal{E}\left(\tau\right)\leq\frac{1}{2\delta_2}B+\frac{V\left(f_{\max}-f_{opt}\right)}{\delta_2} \tag{62}$$

Rearranging (62), we have

$$\lim_{M\to\infty}\frac{1}{MT}\mathbb{E}\sum_{m=1}^{M}\sum_{\tau=(m-1)T+1}^{mT}E\left(\tau\right)\geq E_{max}-\frac{1}{2\delta_2}B-\frac{V\left(f_{\max}-f_{opt}\right)}{\delta_2} \tag{63}$$

Similarly, based on (57), we can obtain

$$\lim_{M\to\infty}\frac{1}{MT}\mathbb{E}\left[\sum_{m=1}^{M}\sum_{\tau=(m-1)T+1}^{mT}f\left(\tau\right)\right]\geq\lim_{M\to\infty}\frac{1}{VMT}\mathbb{E}\left[L\left(MT\right)-L\left(1\right)\right]-\frac{B}{2V}+f_{opt} \tag{64}$$

Since $\lim_{M\to\infty}\frac{1}{VMT}\mathbb{E}\left[L\left(MT\right)-L\left(1\right)\right]=0$, we have

$$\lim_{M\to\infty}\frac{1}{MT}\mathbb{E}\left[\sum_{m=1}^{M}f\left(\tau\right)\right]\geq f_{opt}-\frac{B}{2V} \tag{65}$$

This completes the proof of Theorem 2.

REFERENCES

[1] Z. Zhou, H. Liao, B. Gu, K. M. S. Huq, S. Mumtaz, and J. Rodriguez, "Robust mobile crowd sensing: When deep learning meets edge computing," *IEEE Netw.*, vol. 32, no. 4, pp. 54–60, Jul. 2018.

[2] R. Bolla, R. Bruschi, F. Davoli, and F. Cucchietti, "Energy efficiency in the future Internet: A survey of existing approaches and trends in energy-aware fixed network infrastructures," *IEEE Commun. Surv. Tutor.*, vol. 13, no. 2, pp. 223–244, Jul. 2011.

[3] C. Liu, B. Natarajan, and H. Xia, "Small cell base station sleep strategies for energy efficiency," *IEEE Trans. Veh. Technol.*, vol. 65, no. 3, pp. 1652–1661, Mar. 2016.

[4] A. Orsino, A. Samuylov, D. Moltchanov, S. Andreev, and Y. Koucheryavy, "Time-dependent energy and resource management in mobility-aware D2D-empowered 5G systems," *IEEE Wirel. Commun.*, vol. 24, no. 4, pp. 14–22, 2017.

[5] Y. Chia, S. Sun, and R. Zhang, "Energy cooperation in cellular networks with renewable powered base stations," *IEEE Trans. Wirel. Commun.*, vol. 13, no. 12, pp. 6996–7010, Dec. 2014.

[6] D. Liu, C. Yue, K. K. Chai, and T. Zhang, "Backhaul aware joint uplink and downlink user association for delay-power trade-offs in HetNets with hybrid energy sources," *Trans. Emerg. Telecommun. Technol.*, vol. 28, no. 3, 2015.

[7] I. Ahmed, A. Ikhlef, D. W. K. Ng, and R. Schober, "Power allocation for an energy harvesting transmitter with hybrid energy sources," *IEEE Trans. Wirel. Commun.*, vol. 12, no. 12, pp. 6255–6267, Dec. 2013.

[8] D. Zhang, Y. Qiao, L. She, R. Shen, J. Ren, and Y. Zhang, "Two time-scale resource management for green Internet of things networks," *IEEE Internet Things J.*, vol. 6, no. 1, pp. 545–556, Feb. 2019.

[9] Y. Guo, M. Pan, Y. Fang, and P. P. Khargonekar, "Decentralized coordination of energy utilization for residential households in the smart grid," *IEEE Trans. Smart Grid*, vol. 4, no. 3, pp. 1341–1350, Sep. 2013.

[10] N. Zhang, H. Liang, N. Cheng, Y. Tang, J. W. Mark, and X. S. Shen, "Dynamic spectrum access in multi-channel cognitive radio networks," *IEEE J. Sel. Areas Commun.*, vol. 32, no. 11, pp. 2053–2064, Nov. 2014.

[11] C. K. Ho and R. Zhang, "Optimal energy allocation for wireless communications with energy harvesting constraints," *IEEE Trans. Signal Process.*, vol. 60, no. 9, pp. 4808–4818, Sep. 2012.

[12] S. Zhang, N. Zhang, S. Zhou, J. Gong, Z. Niu, and X. Shen, "Energy-aware traffic offloading for green heterogeneous networks," *IEEE J. Sel. Areas Commun.*, vol. 34, no. 5, pp. 1116–1129, May 2016.

[13] H. Mahdavi-Doost, N. Prasad, and S. Rangarajan, "Optimizing energy efficiency over energy-harvesting LTE cellular networks," *IEEE Transactions on Green Communications and Networking*, vol. 1, no. 3, pp. 320–332, Sep. 2017.

[14] J. Gong, Z. Zhou, and S. Zhou, "On the time scales of energy arrival and channel fading in energy harvesting communications," *IEEE Transactions on Green Communications and Networking*, vol. 2, no. 2, pp. 482–492, Jun. 2018.

[15] D. Liu, Y. Chen, K. K. Chai, T. Zhang, and M. Elkashlan, "Two-dimensional optimization on user association and green energy allocation for HetNets with hybrid energy sources," *IEEE Trans. Commun.*, vol. 63, no. 11, pp. 4111–4124, Nov. 2015.

[16] M. Diehl, R. Amrit, and J. B. Rawlings, "A Lyapunov function for economic optimizing model predictive control," *IEEE Trans. Autom. Control*, vol. 56, no. 3, pp. 703–707, Mar. 2011.

[17] W. Wu, Q. Yang, B. Li, and K. S. Kwak, "Adaptive resource allocation algorithm of Lyapunov optimization for time-varying wireless networks," *IEEE Commun. Lett.*, vol. 20, no. 5, pp. 934–937, May 2016.

[18] Y. Mao, J. Zhang, and K. B. Letaief, "A Lyapunov optimization approach for green cellular networks with hybrid energy supplies," *IEEE J. Sel. Areas Commun.*, vol. 33, no. 12, pp. 2463–2477, Dec. 2015.

[19] Y. Hu, C. Qiu, and Y. Chen, "Lyapunov-optimized two-way relay networks with stochastic energy harvesting," *IEEE Trans. Wirel. Commun.*, vol. 17, no. 9, pp. 6280–6292, Sep. 2018.

[20] Y. Cui, V. K. N. Lau, and F. Zhang, "Grid power-delay tradeoff for energy harvesting wireless communication systems with finite renewable energy storage," *IEEE J. Sel. Areas Commun.*, vol. 33, no. 8, pp. 1651–1666, Aug. 2015.

[21] H. A. Tran, S. Hoceini, A. Mellouk, J. Perez, and S. Zeadally, "QoE-based server selection for content distribution networks," *IEEE Trans. Comput.*, vol. 63, no. 11, pp. 2803–2815, Nov. 2014.

[22] C. E. Shannon, "A mathematical theory of communication," *Bell Syst. Tech. J.*, vol. 27, no. 11, pp. 379–423, 1948.

[23] M. J. Neely, "Stochastic network optimization with application to communication and queueing systems," *Synthesis Lectures on Communication Networks*, vol. 3, no. 1, pp. 1–211, 2010.

[24] W. A. Massey and R. Srinivasan, "A packet delay analysis for cellular digital packet data," *IEEE Journal on Selected Areas in Communications*, vol. 15, no. 7, pp. 1364–1372, 1997.

[25] Y. He, L. Tang, Y. Ren, J. Rodriguez, and S. Mumtaz, "Cross layer resource allocation for multi-hop V2X communications," *Wirel. Commun. Mob. Comput.*, vol. 1, no. 1, pp. 1–1, Feb. 2019.

[26] J. Li, Q. Yang, K. S. Kwak, and R. R. Rao, "Cross-layer resource optimization for wireless relay networks under dynamic node selfishness," *IEEE Trans. Veh. Technol.*, vol. 66, no. 8, pp. 7332–7345, Aug. 2017.

[27] G. Zhang, Y. Chen, Z. Shen, and L. Wang, "Distributed energy management for multi-user mobile-edge computing systems with energy harvesting devices and QoS constraints," *IEEE Internet Things J.*, pp. 1–1, Oct. 2018.

[28] C. Liang, F. R. Yu, H. Yao, and Z. Han, "Virtual resource allocation in information-centric wireless networks with virtualization," *IEEE Trans. Veh. Technol.*, vol. 65, no. 12, pp. 9902–9914, Dec. 2016.

[29] Y. Wang, L. Wu, and S. Wang, "A fully-decentralized consensus-based ADMM approach for DC-OPF with demand response," *IEEE Trans. Smart Grid*, vol. 8, no. 6, pp. 2637–2647, Nov. 2017.

[30] G. Chen and Q. Yang, "An ADMM-based distributed algorithm for economic dispatch in islanded microgrids," *IEEE Trans. Ind. Informat.*, vol. 14, no. 9, pp. 3892–3903, Sep. 2018.

[31] Z. Zhou, P. Liu, J. Feng, Y. Zhang, S. Mumtaz, and J. Rodriguez, "Computation resource allocation and task assignment optimization in vehicular fog computing: A contract-matching approach," *IEEE Trans. Veh. Technol.*, vol. 68, no. 4, pp. 3113–3125, Apr. 2019.

[32] Z. Zhou, C. Gao, X. Chen, Z. Yan, S. Mumtaz, and J. Rodriguez, "Social big-data-based content dissemination in Internet of vehicles," *IEEE Trans. Ind. Inform.*, vol. 14, no. 2, pp. 768–777, Feb. 2018.

[33] S. Boyd, N. Parikh, E. Chu, B. Peleato, and J. Eckstein, "Distributed optimization and statistical learning via the alternating direction method of multipliers," *Foundations and Trends in Machine Learning*, vol. 3, no. 1, p. 1–122, Jan. 2011.

[34] Y. Guo, Q. Yang, and K. S. Kwak, "Quality-oriented rate control and resource allocation in time-varying OFDMA networks," *IEEE Trans. Veh. Technol.*, vol. 66, no. 3, pp. 2324–2338, Mar. 2017.



https://dspace.org/

Two-timescale resource allocation for automated networks in IIoT

He, Yanhua; Ren, Yun; Zhou, Zhenyu; Mumtaz, Shahid; Al-Rubaye, Saba ...

2022-04-04
IEEE
https://doi.org/10.1109/TWC.2022.3162722
He Y, Ren Y, Zhou Z, et al., (2022) Two-timescale resource allocation for automated networks in IIoT. IEEE Transactions on Wireless Communications, Volume 21, Issue 10, October 2022, pp. 7881-7896

Downloaded from a DSpace repository. https://dspace.org/